Journal of Materials Chemistry B

ROYAL SOCIETY OF CHEMISTRY

PAPER

View Article Online
View Journal | View Issue

Check for updates

Cite this: J. Mater. Chem. B, 2025, 13, 10027

Copper oxide nanoparticles as delivery vehicles for different Pt(II)-drugs: experimental and theoretical evaluation†

Shahdan Abdelkareem, [a] Mayyada M.H. El-Sayed, [a] Nahed Yacoub, [a] Aly Reda, [a] Valeria Butera, [b] Matteo Farnesi Camellone, [c] Ida Ritacco *[d] and Tamer Shoeib *[a]

Chemotherapy is a key element in cancer treatment. The first drugs to be clinically used for this purpose were platinum(II) complexes and even today they are highly effective in the treatment of the disease. However, side effects, resulting from their use, limit their clinical usefulness. Furthermore, if administered intravenously into the circulation, platinum(II)-based anticancer medications may cause adverse effects due to interactions with molecules found in human bodies, thus preventing them to reach the final target. Stomach secretions can also destroy them. As a result, their absorption might be restricted, rendering oral delivery ineffective. Over the years, several methodologies were developed to overcome the limits associated with the use of the platinum(II) drugs, including their targeted delivery. In this context, our study proposes copper(II) oxide nanoparticles (CuO NPS) as a promising and excellent carrier of platinum(II)-based anticancer drugs. In this work, we examined the loading efficiency of cisplatin, oxaliplatin and nedaplatin on the surface of CuO nanoparticles by using experimental techniques such as UV-visible spectroscopy, FTIR spectroscopy, the BET method, and XRD, and theoretical ones based on DFT calculations under periodic boundary conditions (PBC). UV-vis spectroscopy determined that cisplatin had the highest entrapment efficiency and loading capacity compared to the other drugs, with 52% entrapment efficacy and an adsorption capacity of 949 mg g^{-1}, indicating a stronger binding with CuO nanoparticles. The experimental results are consistent with DFT simulations indicating that Pt(II)-drugs exhibit favorable adsorption on CuO (111) surfaces, particularly when the Pt(II)-drug is cisplatin. The most stable configurations indicate that cisplatin, nedaplatin, and oxaliplatin prefer to coordinate with the surface tri-coordinated Cu. However, cisplatin has the most intense contact with the copper oxide surface, with an adsorption energy (E_{ads}) of −3.0 eV. Both experimental and theoretical results highlight that CuO nanoparticles are excellent Pt(II) anticancer drug carriers, especially in the case of cisplatin, which undergoes strong interactions with the support, necessary for the delivery phase, and easy desorption, important in the antitumor action phase of the drug.

Received 26th November 2024,
Accepted 8th July 2025

DOI: 10.1039/d4tb02636e

rsc.li/materials-b

Open Access Article. Published on 10 July 2025. Downloaded on 2/8/2026 3:01:31 PM.
This article is licensed under a Creative Commons Attribution 3.0 Unported Licence.

Introduction

The first platinum-based drug used as an antiproliferative agent with high anticancer activity was cisplatin, *cis*-diammine-dichloroplatinum(II).[1] Since the discovery of cisplatin, several Pt(II)-based anticancer drugs have been designed and tested,[2] but to date the most used in clinical therapy together with cisplatin are oxaliplatin and nedaplatin, square-planar d8 platinum(II) complexes that cause cancer cell death by binding to nuclear DNA and distorting its structure.[3] For example, many malignant tumors, including those of the breast,[4] colon,[5] and ovary,[6] respond therapeutically to cisplatin. Nedaplatin has shown positive effects on esophageal cancer and urothelial cancer.[7] Despite their high efficacy, the side effects related to

[a] Department of Chemistry, School of Sciences & Engineering, The American University in Cairo, AUC Avenue, P.O. Box 74, New Cairo 11835, Egypt. E-mail: T.Shoeib@aucegypt.edu
[b] Dipartimento di Scienze e Tecnologie Biologiche, Chimiche e Farmaceutiche, Università di Palermo, viale delle Scienze Edificio 17, 90128 Palermo, Italy
[c] Consiglio Nazionale delle Ricerche-Istituto Officina dei Materiali (CNR-IOM), 34136 Trieste, Italy
[d] Dipartimento di Chimica e Biologia, Università degli Studi di Salerno, via Giovanni Paolo II 132, 84084 Fisciano, Salerno, Italy. E-mail: iritacco@unisa.it

† Electronic supplementary information (ESI) available. See DOI: https://doi.org/10.1039/d4tb02636e

Open Access Article. Published on 10 July 2025. Downloaded on 2/8/2026 3:01:31 PM. This article is licensed under a Creative Commons Attribution 3.0 Unported Licence.

these cytotoxic agents, which include lack of selectivity, significant systemic toxicity, and drug resistance, limit their clinical use.[8] Furthermore, if administered orally, Pt(II) complexes could be degraded by gastric juices, while if injected intravenously they could react with the numerous molecules present in our body, preventing them from reaching the final target.[9–12] To overcome the drawbacks arising from the use of Pt(II)-based anticancer drugs, efforts have been devoted to developing new methods, including the use of 'prodrugs' with platinum in the more inert +IV oxidation state,[12,13] or the use of nanoparticles as drug delivery systems to improve the efficacy and safety of Pt(II) chemotherapy drugs.[14] In the latter methodology, the idea is to adsorb the Pt(II) drugs on the surface of nanoparticles, such as those of copper oxide (CuO), which appear to be promising in drug delivery applications due to their unique properties. In fact, CuO nanoparticles feature distinctive morphological structures, specific physical and chemical characteristics, such as their high surface area-to-volume ratio and variable surface chemistry, which make them ideal for drug delivery and adsorption.[15,16] Copper oxide nanoparticles (CuO NPs) have emerged as a highly promising therapeutic platform, demonstrating dual functionality in both cancer treatment and antimicrobial applications. Their anticancer potential has been validated across multiple cancer types, including breast, kidney, lung, and prostate malignancies.[17,18] Beyond their direct cytotoxic effects, these nanoparticles serve as efficient drug delivery vehicles, enhancing targeted therapy in nanomedical applications.[17,18] The biomedical utility of CuO NPs extends to their remarkable antimicrobial properties, which have led to their increasing adoption in clinical settings.[19] These nanoparticles display broad-spectrum antibacterial activity against both Gram-positive and Gram-negative bacterial strains, making them particularly valuable for advanced wound care applications.[20] This enhanced antibacterial performance stems from their unique physicochemical characteristics, including nanoscale dimensions, exceptional surface area-to-volume ratio, inherent biocompatibility, and heightened chemical reactivity.[21]

Notably, biologically synthesized CuO NPs have shown pronounced antifungal efficacy against clinically relevant fungal pathogens such as *Penicillium citrinum*, *Aspergillus niger*, *Fusarium oxysporum*, and *Alternaria solani.*[22] The antimicrobial mechanism of action, common to both antibacterial and antifungal effects, involves the generation of reactive oxygen species (ROS).[23,24] These ROS induce oxidative damage to microbial cell structures, compromising membrane integrity and ultimately leading to cellular apoptosis.[23,24] While the ROS-generating capacity of CuO NPs offers significant therapeutic potential, their potential cytotoxicity necessitates careful evaluation for biomedical applications. The primary mechanism of toxicity involves ROS-mediated oxidative stress, which can induce DNA damage and impair cellular function. Key physicochemical parameters governing toxicity include particle size, surface characteristics, dosage, and exposure duration.[25] Toxicity modulation studies reveal that sub-40 nm CuO NPs exhibit enhanced cellular penetration, leading to greater ROS production and genotoxic effects. Comparative analyses show 24 nm particles generate 72% more ROS than those of 33 nm within one hour of exposure.[26,27] Dose optimization strategies demonstrate that fractionated administration reduces hepatotoxicity markers significantly compared to single-dose delivery.[8]

Advanced surface engineering approaches have successfully mitigated toxicity concerns while preserving therapeutic efficacy, and PEGylation of 30 nm CuO NPs was shown to reduce macrophage ROS production by 60% without compromising anticancer activity.[14] Similarly, Moringa oleifera-synthesized CuO NPs at 66.89 nm, incorporated in polyacrolein matrices, exhibit selective cytotoxicity, eliminating cancer cells while maintaining $>85\%$ viability in normal dermal fibroblasts.[28] Crystallinity studies indicate that defect-free crystalline CuO NPs induce less oxidative stress than their defective counterparts, regardless of size.[27] Innovative composite materials further enhance biocompatibility; cellulose–chitosan matrices containing ≤ 35 nmol mg^{-1} CuO NPs retain potent antibacterial effects while showing minimal cytotoxicity to human cells.[29] These findings underscore the critical importance of nanomaterial design and parameter optimization in developing safe, effective CuO NP-based therapies. Comprehensive characterization of the physicochemical properties and strategic surface modifications remain essential for advancing their biomedical applications.

Copper oxide nanoparticles can interact with drugs using a variety of processes, including electrostatic interactions, hydrogen bonding, and van der Waals forces[30] that depend on the physicochemical properties of the drug molecules and the surface characteristics of the nanoparticles. In addition to non-covalent interactions, CuO nanoparticles can establish strong coordination interactions with Pt(II) drugs. Surface oxygen atoms in CuO NPs can function as electron donors, allowing the creation of coordination complexes with platinum centers, which might improve the adsorption stability and potentially influence drug release patterns.[31] The strength of these interactions is strongly dependent on environmental factors. For example, at lower pH levels enhanced protonation of the CuO NPs surfaces can change both the amount of coordination and the electrostatic interactions, impacting the adsorption and release of Pt(II) drugs.[32] Solvent polarity also greatly influences interactions of the Pt(II) drug and CuO NPs with protic solvents competing for coordination sites on the CuO NP surfaces. While leakage of Cu^{2+} may occur under physiological circumstances, undermining both complex stability and safety, surface changes of the CuO NPs such as those resulting from PEGylation efficiently decrease Cu^{2+} release while increasing colloidal stability. Understanding the coordination, environmental, and leaching characteristics is essential for creating viable CuO NP based drug delivery systems.[25,33]

Drug adsorption on the copper oxide nanoparticles has various benefits, such as the possibility to preserve the drugs from deterioration and increasing their stability. Adsorption on CuO nanoparticles can also increase the solubility and the bioavailability of poorly soluble medicines, improving their therapeutic effectiveness. Some studies have investigated the use of oxides nanoparticles as carriers for Pt(II)-based drugs. Despite significant studies on other metal oxides such as iron

 This journal is © The Royal Society of Chemistry 2025

Open Access Article. Published on 10 July 2025. Downloaded on 2/8/2026 3:01:31 PM. This article is licensed under a Creative Commons Attribution 3.0 Unported Licence.

oxide, titanium dioxide, and zinc oxide, few studies have examined the usage of CuO NPs in platinum-based anticancer treatment options.

CuO NPs offer some advantages over other metal oxide nanoparticles such as ZnO and TiO_2, particularly in biomedical and antimicrobial applications. CuO NPs showcase strong antimicrobial properties owing to their capability to produce reactive oxygen species (ROS) and disturb microbial cell membranes, rendering them highly efficient against a wide range of bacteria and fungi.[34] While ZnO NPs operate primarily *via* the release of Zn^{2+} ions and the generation of ROS, demonstrating effectiveness against Gram-positive bacteria, they lack efficacy towards Gram-negative bacteria.[35,36] In contrast, titanium dioxide nanoparticles (TiO_2NPs) need to be activated by ultraviolet (UV) light in order to produce ROS and demonstrate antimicrobial advantages. However, reliance on UV activation restricts their practical application.[37,38] Comparative studies between CuO NPs and iron oxide nanoparticles, Fe_2O_3 NPs, reveal superior antimicrobial efficacy for CuO NPs against multidrug-resistant pathogens. When tested against clinically relevant strains, CuO NPs demonstrated significantly larger inhibition zones compared to their iron oxide counterparts: 22 ± 1 mm *versus* 14 ± 1 mm for methicillin-resistant *Staphylococcus aureus* (MRSA), and 18 ± 1 mm *versus* 12 ± 1 mm for *Escherichia coli*. These findings clearly establish the enhanced antibacterial potential of CuO NPs against both Gram-positive and Gram-negative resistant bacterial strains.[39]

Systematic comparative studies examining the interaction mechanisms between different Pt(II) drugs and CuO nanoparticles remain limited. While previous research has demonstrated the potential of metal oxide nanoparticles for platinum drug delivery, there is still an insufficient understanding of the specific physicochemical factors that influence the loading efficiency and release profile of different Pt(II) drugs on CuO NPs. In recent years, some studies have explored the use of CuO and other copper-based nanoparticles as nanocarriers for platinum(II) anticancer drugs – particularly cisplatin – demonstrating high entrapment efficiencies, improved loading capacities, and enhanced cytotoxicity compared to free drugs or conventional formulations.[40,41] For example, PEGylated chitosan nanoparticles loaded with nedaplatin or oxaliplatin showed significantly increased cytotoxic activity against cancer cells, attributed to improved drug retention and cellular uptake.[41] Other nanocarrier systems, such as liposomes, polymeric micelles, and mesoporous silica nanoparticles, have also been developed to address the limitations of platinum-based chemotherapy, including poor solubility, rapid systemic clearance, and dose-limiting toxicities.[8] This study addresses this knowledge gap by providing a comprehensive analysis of three clinically relevant Pt(II) drugs which are cisplatin, oxaliplatin, and nedaplatin on CuO nanoparticles, combining multiple characterization techniques with computational modeling to elucidate structure–property relationships that govern drug–nanoparticle interactions. The drug–CuO systems will be first characterized using Fourier transform infrared (FTIR) spectroscopy and X-ray diffraction (XRD) to confirm loading of each of the three drugs. The Brunauer–Emmett–Teller (BET) method will be used to determine the specific surface area and the total pore volume of the loaded CuO nanoparticles. With the aid of UV-Visible spectrophotometric measurements, the entrapment efficiency and adsorption capacities of the nanoparticles for Pt(II)-drugs will be estimated to conclude which drug has the best adsorption capacity on the surface of the CuO nanoparticles. To support the experimental data, DFT calculations will be performed on the different Pt(II)–CuO systems, allowing us (i) to quantify the drug–carrier interaction, in terms of adsorption energy (E_{ads}, eV) and (ii) to define the most stable coordination modes of each drug. We expect that CuO nanoparticles would have different adsorption capabilities and coordination interactions with different Pt(II) drugs, resulting in measurable changes in drug loading efficiency and stability. We anticipate that our findings will shed light on the feasibility of CuO NPs as carriers for platinum-based anticancer drugs, as well as give insights into how to optimize their design for drug delivery applications.

Experimental section

Materials

99.9% Oxaliplatin, 99.9% cisplatin, and 99.8% nedaplatin were sourced from Shandong Boyuan Pharmaceutical Co., Ltd (Shandong, China). Copper oxide nanoparticles of particle size $<50 \pm 7$ nm (as measured by TEM) were purchased from NanoTech (Cairo, Egypt).

Methods

150 mg nedaplatin, 35 mg oxaliplatin, and 12 mg cisplatin were dissolved each in 5 mL of deionized water. The solutions were then stirred until completely dissolved. Copper oxide nanoparticles were soaked in the saturated solutions of the drugs, with a ratio of 2 : 1 (m m^{-1}), for 48 hours while stirring at 300 rpm, and the solution was kept in the dark. The solutions were then centrifuged at 4000 rpm for 30 minutes and the supernatant was used to perform quantitative analysis using UV-visible spectroscopy. The same steps were repeated and the solutions of the copper oxide nanoparticles with the drugs were left for 16 hours with stirring at 300 rpm and at 35 °C until complete evaporation. The drug-loaded powder was stored at 4 °C.[42] The powder was then used to conduct different characterization.

Characterization

The dry powders of the CuO nanoparticles were examined for their crystallinity and composition before and after the loading of the three Pt(II)-drugs using a Bruker D8 Discover Diffractometer. The functional groups present in the CuO nanoparticles, and the three samples of the loaded drugs were determined using Fourier transform infrared spectroscopy. The peaks were also compared as an initial confirmation of the loading process. To prepare the samples, they were thoroughly mixed with potassium bromide (KBr) at a 1 : 100 ratio (sample : KBr) using

Open Access Article. Published on 10 July 2025. Downloaded on 2/8/2026 3:01:31 PM.
This article is licensed under a Creative Commons Attribution 3.0 Unported Licence.

an agate mortar and pestle to ensure homogeneity. The mixture was pressed into transparent pellets at 15 000 PSI under anhydrous conditions, preventing moisture-related artifacts and analyzed using a Nicolet 380 FT-IR Spectrometer with a wavelength range of 500 to 4000 cm^{-1}. This protocol aligns with literature recommendations for reproducible KBr pellet preparation.[43,44] The surface charge of CuO nanoparticles was evaluated by dynamic light scattering (DLS) with a Zetasizer Nano ZS90 (Malvern Instruments, UK) at 25 °C, resulting in a slightly negative zeta potential of −17.7 mV. The measurements were taken in a 1 : 10 (v/v) dilution of ultrapure water.

Determination of the surface area and porosity

The textural properties of CuO NPs were measured before and after loading of the Pt(II)-drugs. Specific surface areas and pore size distributions were determined by measuring the N_2 adsorption–desorption isotherms of the unloaded nanoparticles and the drug-loaded nanoparticles, at 77 K on a Micrometrics ASAP 2020 apparatus. Before measurement, the CuO NPs and the loaded nanoparticles were degassed at 40 °C for 6 h under vacuum (10 mHg). Surface areas and pore size distributions were calculated using the BET and BJH (Barrett–Joyner–Halenda) methods.

Determination of loading capacity

The platinum-based drugs, with quantities adjusted based on solubility, were dissolved in 5 mL distilled water in the following quantities 12 mg, 150 mg, 35 mg for cisplatin, nedaplatin, and oxaliplatin, respectively.[45–47] CuO NPs were introduced to each drug solution in a 2 : 1 ratio (m m^{-1}). The solutions were allowed to soak at room temperature for 48 hours to allow for adequate drug–CuO nanoparticle interactions. After soaking, the solutions were centrifuged at 4000 rpm for 30 minutes to free the non-interacted nanoparticles from the drug-loaded solution. The decant was carefully extracted to conduct spectrophotometric analysis (Carry 3500 UV-vis, model no. G9864A, Mulgrave VIC 3170, Australia). The peaks were detected in the range of 200–230 nm. A five-point calibration curve for each drug was constructed as shown in Fig. S1–S3 of the ESI.† The entrapment efficiency (EE%) and the adsorption capacity were calculated. Using the following equations:

$$\text{Entrapment efficiency (EE\%)} = (\text{the amount of substance entrapped/the total substance amount}) \times 100$$

$$\text{Adsorption capacity} = (\text{initial drug concentration} - \text{drug concentration after adsorption}) \times \text{volume of solution/mass of the adsorbent}$$

Computational details

DFT calculations were performed within Periodic Boundary Conditions (PBC) using the Perdew–Burke–Ernzerhof (PBE) exchange–correlation functional based on the generalized gradient approximation (GGA)[48] and ultrasoft pseudopotentials.[49] The spin polarized Kohn–Sham equations were solved in the plane wave pseudopotential framework, with the wavefunction basis set and the Fourier representation of the charge density being limited by kinetic cutoffs of 60 and 480 Ry, respectively, chosen after having performed the appropriate convergence tests. Additionally, we set the force threshold to 10^{-3} Ry $Bohr^{-1}$, ensuring that further reductions in the threshold did not lead to any significant changes in the total energy. The Quantum Expresso code[50] was employed for all calculations.

Based on our XRD experimental studies (Fig. 1) and previously reported theoretical data,[51] the interaction between Pt(II)-drugs and CuO nanoparticles was investigated by using the thermodynamically most stable non polar termination of CuO surface, *i.e.* CuO(111). In fact, close-packed surfaces can be considered good models for the description of nanoparticles.

In this study, a CuO(111) surface was built starting from the CuO bulk, which has a monoclinic crystal structure with *C*2/*c* symmetry.[52] To verify the reliability of the model and the selected calculation parameters, the lattice constants of the CuO bulk were calculated and compared with the experimental data. The computed lattice parameters of the CuO bulk monoclinic unit cell (a = 4.779 Å, b = 3.423 Å, c = 5.129 Å and b = 99.54°) are in good agreement with the experimental values (a = 4.682 Å, b = 3.424 Å, c = 5.127 Å and b = 99.42°).[53]

After extensive convergence tests, based on the size of Pt(II) substrates, and in order to minimize interactions between the periodic slabs, CuO(111) was modeled as a 3 × 3 periodic supercell with a separation of more than 10 Å between replicas along the x and y directions. In addition, according to preliminary tests and the literature,[54–56] we chose to use a supercell consisting of four layers with a vacuum separation of 23 Å along the z direction perpendicular to the surface (Fig. 2).

During the calculations, the two bottom layers of the surface were constrained to their equilibrium bulk-like positions, while the upper ones and the Pt-drugs were fully relaxed. In addition, CuO(111) was modeled in the bulk-like spin ordering since, as the literature suggests, it is the most stable among the three possible ones.[57] The threshold for energy convergence was set

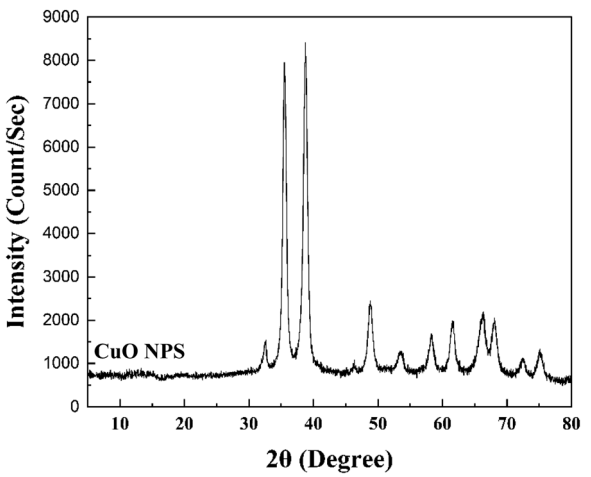

Fig. 1 XRD pattern of CuO NPs.

 This journal is © The Royal Society of Chemistry 2025

Open Access Article. Published on 10 July 2025. Downloaded on 2/8/2026 3:01:31 PM.
This article is licensed under a Creative Commons Attribution 3.0 Unported Licence.

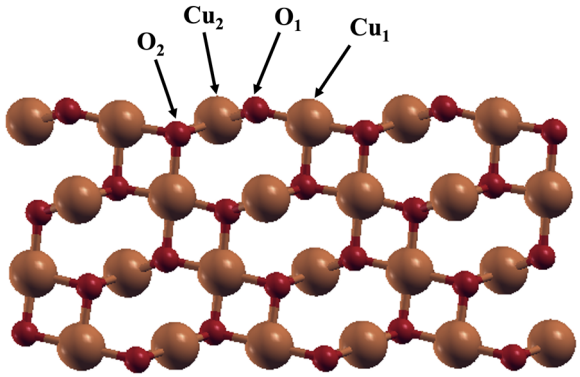

Fig. 2 Optimized structure of the CuO(111) surface. Cu and O atoms are represented using a ball and stick model and depicted in auburn and red, respectively. The top layer consists of tri- and four-coordinated Cu and O atoms. Tri-coordinated O atoms (O_1) are the most exposed atoms. O_1 are connected to one tri-coordinated and two tetra-coordinated copper atoms, defined in Fig. 2, Cu_1 and Cu_2, respectively. Cu_1 is coordinatively unsaturated, whereas Cu_2 is coordinatively saturated. O_2 are tetra-coordinated subsurface oxygen atoms, and they are connected to two Cu_2, to one Cu_1 and to one Cu atom of the second layer.

to 10^{-6} eV and due to the large dimension of the systems Γ points were used for the Brillouin zone integration. In addition, the van der Waals (vdW) interactions were explicitly considered employing the zero damping DFT-D3 method of Grimme.[58]

The adsorption energy of the Pt(II)-drugs was computed by using eqn (1):

$$E_{ads} = E_{Pt(II)\text{-drugs@CuO(111)}} - (E_{CuO(111)} + E_{Pt(II)\text{-drugs}}) \quad (1)$$

where, $E_{Pt(II)\text{-drugs@CuO(111)}}$ is the energy of the combined system (namely the surface plus the Pt(II)-drugs), $E_{CuO(111)}$ is the energy of the stoichiometric CuO(111) surface, and $E_{Pt(II)\text{-drugs}}$ is the energy of the Pt(II)-drugs in the gas phase.

The charge transfers are very important to understand the interaction between the drugs and the support. Therefore, the charge analysis was performed following Bader's theory since the charge enclosed within the Bader volume can be considered a good approximation of the total electronic charge of an atom.[59–61] The differences between the Bader charges of the coordinated and gas phase Pt(II)-drugs were calculated according to the equation $\Delta q = \Sigma_{q(Pt(II)@CuO(111))} - \Sigma_{q(Pt(II))}$, where $\Sigma_{q(Pt(II)@CuO(111))}$ is the sum of the Bader charges of cisplatin, nedaplatin and oxaliplatin adsorbed on the CuO(111) surface, while $\Sigma_{q(Pt(II))}$ is the sum of the free Pt(II)-drugs.

Results and discussion

In this work, experimental and theoretical studies were performed to demonstrate the validity of the copper oxide (CuO) nanoparticles as nanocarriers of Pt(II)-based anticancer drugs and to further understand the structural and electronic interactions underlying the binding between Pt(II)-drugs and the CuO carrier. Therefore, X-ray diffraction analysis was carried out to observe the crystal structure of the nanoparticles of copper oxide and to confirm the phase purity, whereas the surface interactions and the drugs adsorption were analyzed through FTIR spectroscopy and DFT calculations. The latter were performed to better investigate the most stable configurations of the Pt(II)-drugs on the surface of the CuO nanoparticles with the corresponding adsorption energies (E_{ads}, eV) in order to provide more details on the interaction between CuO and the Pt(II) anticancer drugs.

X-ray diffraction analysis

The XRD diffraction pattern for the commercial copper oxide nanoparticles is shown in Fig. 1. The spectrum shows distinctive diffraction peaks at 2θ values of 38.7, 35.5, 48.7, 66.4, and 68.1° which match the crystallographic planes of (111), (−111), (−202), (−311), and (220) that correspond to the presence of CuO II, as per the International Center for Diffraction Data (ICDD) pattern of standard copper oxide (JCPDS 48-1548). The highest peak at 2θ of 38.7° corresponds to the crystal lattice of the (111) plane. The average crystallite size of the MSW used was calculated by the Debye–Scherer equation[62] using values of 1.54 Å and 0.9 for the X-ray wavelength and dimensionless form factor K, respectively, and found to be 14.84 nm.[63] Other studies have also reported major peaks for CuO nanoparticles between 35° and 39°,[64,65] confirming the similarity between the findings of this study and the findings reported in the literature. To further assess the structural integrity and crystallinity of the CuO nanoparticles after drug loading, X-ray diffraction (XRD) patterns of CuO NPs loaded with cisplatin, oxaliplatin, and nedaplatin were recorded and are presented in the ESI† (Fig. S4). All drug-loaded samples retain the characteristic diffraction peaks of monoclinic CuO, indicating that the crystal structure of the nanoparticles remains intact following drug incorporation. Furthermore, a slight broadening and reduction in intensity of the main CuO peaks were noted after drug loading, which may be attributed to partial surface coverage by the drugs and a modest decrease in the crystallite size. These results confirm that the post-loading strategy preserves the structural features of CuO NPs while enabling efficient drug incorporation.

FTIR spectroscopy

FTIR spectroscopy was carried out to confirm the adsorption of the drugs on the surface of the CuO nanoparticles. The FTIR analysis results related to the Pt(II)-drugs, the free CuO nanoparticles, and drug–CuO complexes are reported in Fig. 3 (panels A–C). The FTIR spectrum of the free CuO nanoparticles (red line in Fig. 3A–C) shows a broad absorption band around 3500 cm^{-1} which corresponds to the OH functional group. Another band is shown around 1600 cm^{-1} and it corresponds to the aromatic bending of alkenes (C=C). Small peaks from 500 to 900 cm^{-1} are assigned to the bending vibrations of the CuO bond.[66] The FTIR spectrum of the free cisplatin (black line in Fig. 3A) exhibits the characteristic peaks of amine bending at around 1250 cm^{-1} and the typical amine stretching mode shown between 3200 and 3500 cm^{-1} which agrees with the FTIR spectrum of cisplatin previously reported in the literature,[67] whereas free nedaplatin shows peaks of amine stretching from 3000 to 3200 cm^{-1} and the typical bending of

Open Access Article. Published on 10 July 2025. Downloaded on 2/8/2026 3:01:31 PM.
This article is licensed under a Creative Commons Attribution 3.0 Unported Licence.

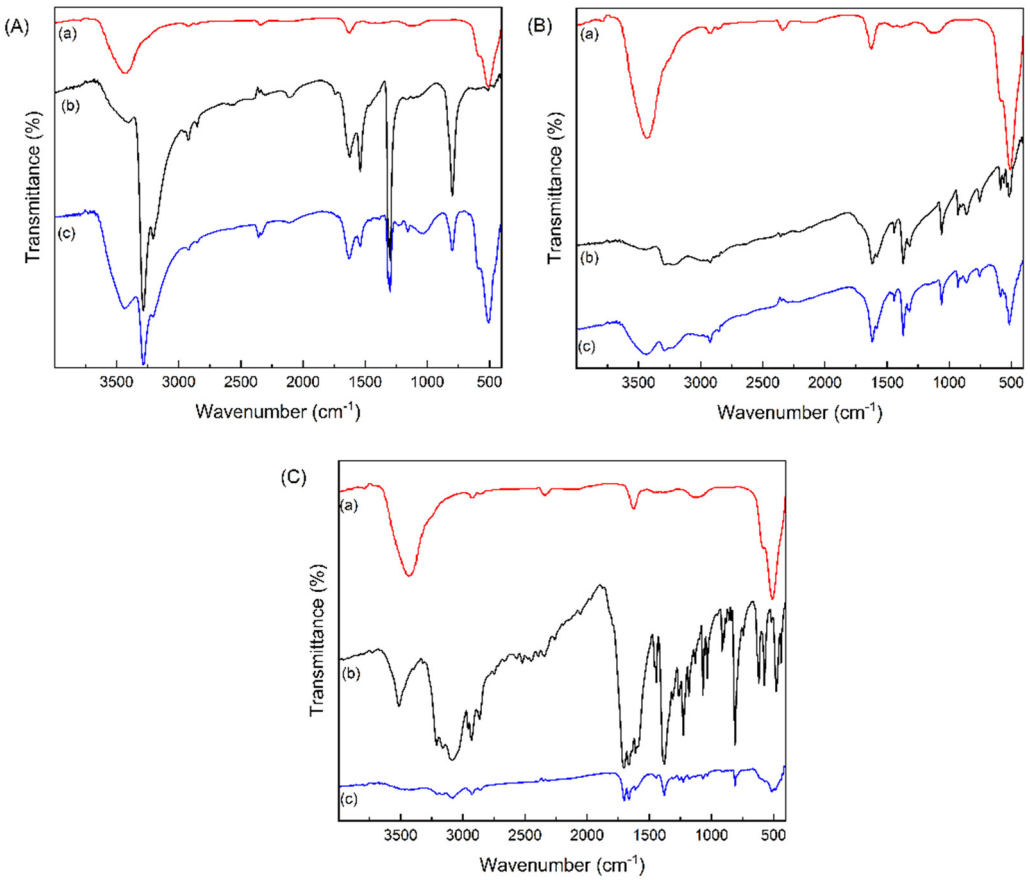

Fig. 3 FTIR spectrum of the free CuO nanoparticles (red line a in panels A–C), the free Pt(II)-drugs (black line b in panels A–C) and the Pt(II)-drugs@CuO complexes (blue lines (c) in panels A, B and C for cisplatin, nedaplatin and oxaliplatin, respectively).

amines at around 1600 cm^{-1} (black line in Fig. 3B).[68] The FTIR spectrum of the oxaliplatin drug (black line in Fig. 3C) shows peaks from 3000 to 3500 cm^{-1} indicating the presence of an N–H stretch as reported in previous literature.[69]

The intensity of the Cisplatin's peak at 3300 cm^{-1} decreases after the interaction and binding to CuO NPS in the complex (blue line in Fig. 3A). This demonstrates the interaction between the CuO NPS and the amine groups of the cisplatin drug. In Nedaplatin, the peak around 3300–3400 cm^{-1} shifts after the binding to the CuO NPs suggesting changes in hydrogen bonding or coordination (blue line in Fig. 3B). Oxaliplatin's wide peak around 3000 cm^{-1} to 3500 cm^{-1} shows a shift, also, demonstrating contact between its amine or hydroxyl groups and the CuO surface (blue line in Fig. 3C). FTIR changes in the 600–700 cm^{-1} range reflect ligand-specific vibrations (C–C stretching in oxaliplatin, NH_3 rocking in cisplatin/nedaplatin) and CuO surface coordination effects. These assignments align with literature reports for platinum–drug ligand[70] and nanoparticle interactions.[71]

Scanning electron microscopy (SEM)

The morphology and particle size of the synthesized CuO nanoparticles were examined by scanning electron microscopy (SEM), as shown in Fig. 4. The SEM image reveals that the CuO nanoparticles are nearly spherical and moderately

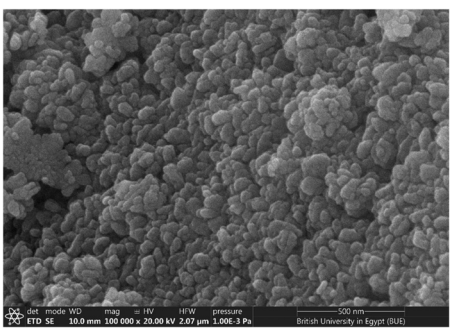

Fig. 4 SEM of copper oxide nanoparticles.

agglomerated, with individual particle sizes ranging from approximately 20 to 55 nm. This observation is consistent with previous reports on the CuO nanoparticle morphology, which often describes aggregated, quasi-spherical particles in this size range.[72,73] The measured particle sizes from SEM are in good agreement with the crystallite sizes determined by XRD, confirming the successful synthesis of nanoscale CuO.

Surface characteristics and interactions

BET analysis was conducted to determine the specific surface area and pore size distribution of the CuO nanoparticles before

 This journal is © The Royal Society of Chemistry 2025

Open Access Article. Published on 10 July 2025. Downloaded on 2/8/2026 3:01:31 PM.
This article is licensed under a Creative Commons Attribution 3.0 Unported Licence.

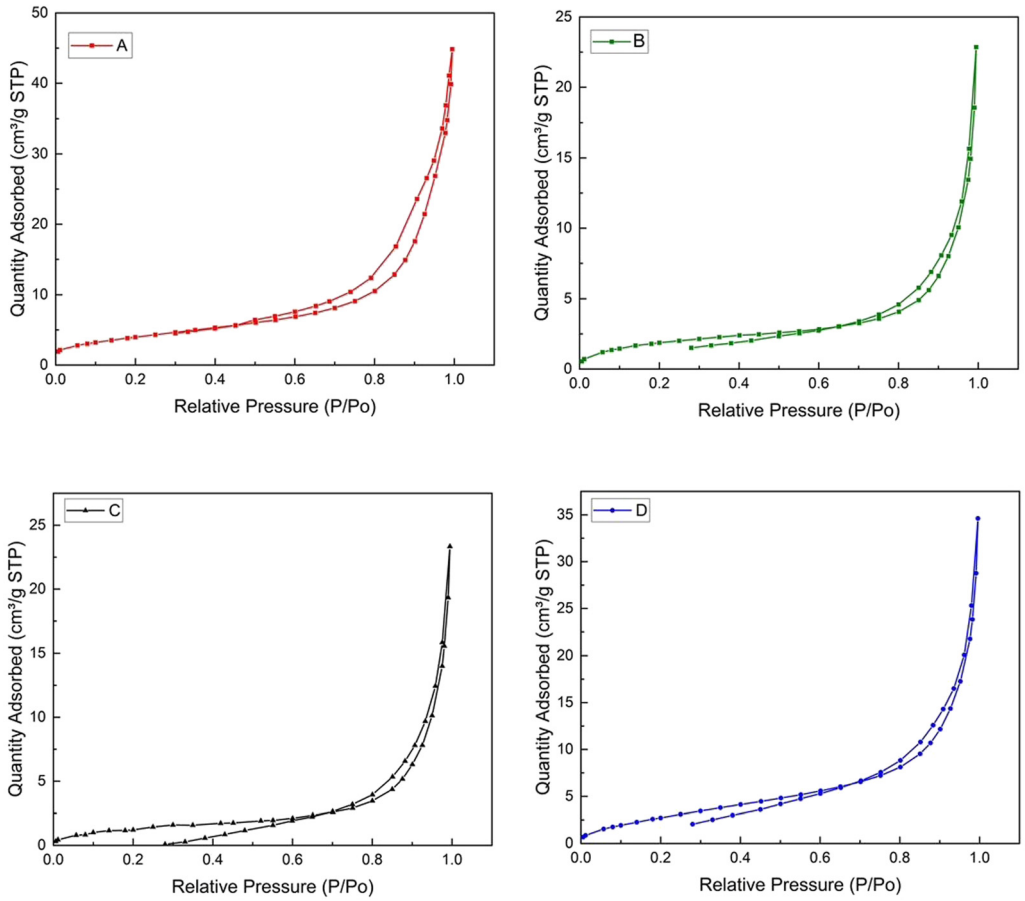

Fig. 5 Nitrogen adsorption–desorption isotherms for (A) free CuO nanoparticles, (B), *cis*@CuO, (C) neda@CuO, and (D) oxa@CuO.

and after binding of the Pt(II)-drugs on their surface. Four materials were analyzed, free CuO nanoparticles, *cis*@CuO, neda@CuO and oxa@CuO. The BET isotherms pertaining to the four materials are depicted in Fig. 5, manifesting type IV isotherms according to the IUPAC classification. These isotherms indicate mesoporosity with pore size ranging from 2–50 nm.[74]

The graph in Fig. 6 shows the BET surface area and the BJH adsorption cumulative surface area of the pores of the copper oxide nanoparticles before and after loading the cisplatin, the nedaplatin and the oxaliplatin drugs. The surface area of pores decreased the most when the cisplatin and the oxaliplatin were loaded on the surface of the copper oxide nanoparticles. When adding the nedaplatin drug to the CuO nanoparticles, the pore surface area did not show a big difference. All CuO samples showed Type IV nitrogen adsorption–desorption isotherms, which are typical of mesoporous materials and include a hysteresis loop caused by capillary condensation within the pores. The free CuO nanoparticles demonstrated an H1-type hysteresis loop, indicating homogeneous, cylindrical mesopores with little network effects. The hysteresis loop switched to H2-type after loading with cisplatin or oxaliplatin, indicating more complex pore structures and pore-blocking effects, which is consistent with drug molecules occupying pore channels. In contrast, nedaplatin-loaded CuO preserved the H1-like hysteresis, indicating that the pore structure remained substantially unaltered and that nedaplatin adsorption took place mostly on the exterior surface rather than within the pores.

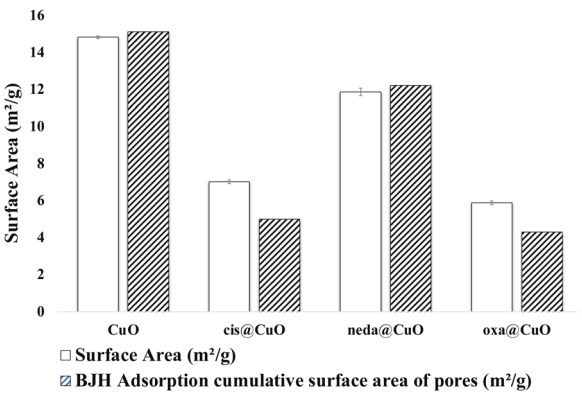

Fig. 6 The BET surface area of the copper oxide nanoparticles before and after adding the Pt-drugs.

In contrast to cisplatin's pore-filling mechanism (−3.0 eV), the surface adsorption of nedaplatin is driven by weak interactions (DFT: −2.6 eV) accounting for its little pore volume change (Fig. 8) and low EE% (21.7%). Although surface adsorption prevents pore occlusion, it reduces drug retention, which explains why nedaplatin is less effective as a carrier than cisplatin/oxaliplatin.

Open Access Article. Published on 10 July 2025. Downloaded on 2/8/2026 3:01:31 PM.
This article is licensed under a Creative Commons Attribution 3.0 Unported Licence.

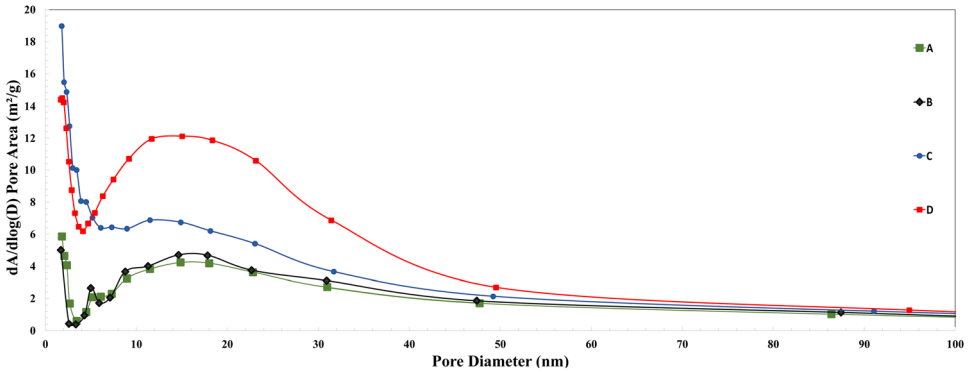

Fig. 7 BJH pore size distributions shown using (A), (B) and (C) correspond to the samples *cis*@CuO, neda@CuO and oxa@CuO, respectively, whereas (D) corresponds to the free CuO nanoparticles.

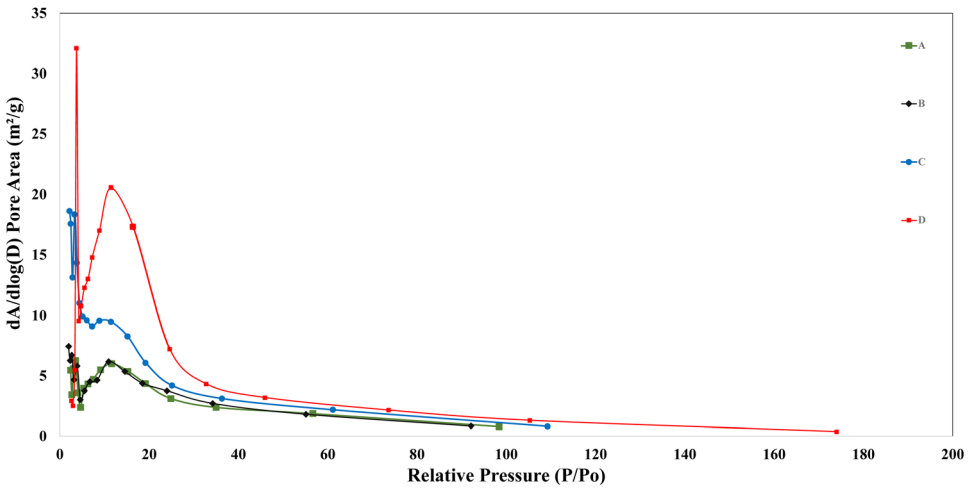

Fig. 8 BJH desorption d*A*/d log(*D*) pore area *vs* relative pressure curves. (A)–(C) correspond to the samples cis@CuO, neda@CuO and oxa@CuO, respectively, whereas (D) is to the free CuO nanoparticles.

The BJH pore size distribution profiles as estimated from the adsorption and desorption branches are demonstrated in Fig. 7 and 8, respectively. Clearly, most pores span the mesoporous size range of 2–50 nm which is consistent with the type IV isotherms.

The total pore volume was also analyzed for the free CuO nanoparticles and when it is loaded with the Pt(II)-drugs as shown in Fig. 9.

The total pore volume of the CuO nanoparticles decreased after binding the drugs implying the filling of their pores with the drug, and nedaplatin shows the least change before and after binding confirming that the CuO NPs are not its best carrier. While both cisplatin and oxaliplatin showed good compatibility with the CuO NPS with no big difference in the pore size volume which is 0.028 $cm^3\ g^{-1}$ and 0.024 $cm^3\ g^{-1}$ for cisplatin and oxaliplatin, respectively.

UV-vis spectroscopy for loading analysis

UV-vis spectroscopy analysis was carried out to obtain quantitative data for the adsorption of the Pt(II)-drugs on the surface of CuO nanoparticles. The adsorption of the cisplatin, oxaliplatin, nedaplatin, and carboplatin drugs occurred in the wavelength range of 200–230 nm in agreement with what was previously reported in the literature.[14,75] Calibration curves for each drug were constructed and the entrapment efficiency and loading capacity were calculated. The entrapment efficiency (EE%) is the proportion of a material that is successfully entrapped or encapsulated within a carrier system, such as nanoparticles in this case.[76] Entrapment efficiency is an essential characteristic in drug delivery systems since it impacts the carrier's success in delivering the targeted material to the target site. It is often used to evaluate the performance of encapsulation methods as well as the carrier system's quality. The following formula is commonly used to calculate entrapment efficiency:[77]

$$\text{Entrapment efficiency (EE)} = (\text{the amount of substance entrapped/the total substance amount}) \times 100$$

The adsorption capacity was also calculated to obtain the amount of Pt(II)-drugs loaded on 1 g of CuO nanoparticles. The loading capacity determines the maximum amount of a drug that can be loaded into the nanoparticles. The entrapment efficiency and the loading capacity were calculated as

 This journal is © The Royal Society of Chemistry 2025

Open Access Article. Published on 10 July 2025. Downloaded on 2/8/2026 3:01:31 PM.
This article is licensed under a Creative Commons Attribution 3.0 Unported Licence.

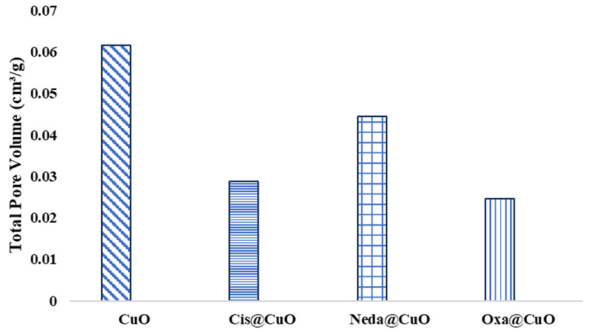

Fig. 9 Total pore volume of the CuO NPs before and after loading of Pt-drugs.

Table 1 Interactions of Pt-drugs with CuO nanoparticles

	Cisplatin	Oxaliplatin	Nedaplatin
Entrapment efficiency (EE%)	52%	38%	13%
Adsorption capacity	949 mg g^{-1}	878 mg g^{-1}	236 mg g^{-1}

shown in the Methods section and the results are shown in Table 1.

The interaction of Pt(II)-drugs with CuO nanoparticles indicates a high possibility of enhancing drug delivery systems in treatment applications. The encapsulation and adsorption of the Pt(II)-drugs have a significant impact on their efficacy. Cisplatin exhibited the highest entrapment efficiency (EE%) of 52%, suggesting that more than its half was effectively contained in the CuO nanoparticles. This high EE% is crucial because it indicates that more of the drug is maintained inside the nanoparticle system, lowering drug loss throughout the entire process of encapsulation. The higher EE% indicates that more of the medicine will be accessible for release at the intended location, thereby increasing the overall treatment effect. This is especially important in cancer treatment as it can help reduce systemic adverse effects. Cisplatin also had the maximum adsorption capacity (949 mg g^{-1}), indicating the amount of loaded cisplatin drug onto the CuO nanoparticles. A better adsorption capacity allows the carrier to carry more drug quantity, greatly increasing therapeutic efficacy, particularly in aggressive cancer therapy where higher drug dosages are frequently required. Cisplatin's high EE% and adsorption capability make it a tempting candidate for drug delivery systems using nanoparticles. The introduction of CuO nanoparticles may improve cisplatin stability and bioavailability, hence increasing its efficacy in cancer treatment. When compared to values reported in the literature for similar systems, the EE% and adsorption capacity achieved for cisplatin in this study are notably competitive. For example, cisplatin-loaded PLGA-mPEG nanoparticles typically show EE% values in the range of 30–40% and adsorption capacities around 200 mg g^{-1},[42] while PBCA nanoparticles show EE% as low as 23%.[67] Mesoporous silica carriers generally show EE% between 45–75% and adsorption capacities below 900 mg g^{-1} for platinum drugs, depending on the drug and the specific functionalization of the silica surface.[78,79] Notably, some advanced polymeric systems can show higher EE% (up to 72%),[42] but often with lower adsorption capacities or more complex synthesis steps. Thus, the CuO nanocarrier system presented here offers a distinct advantage for cisplatin delivery, combining moderate-to-high EE% with exceptionally high adsorption capacity.

For oxaliplatin, the observed EE% (38%) and adsorption capacity (878 mg g^{-1}) are also strong compared to 15% as reported in literature,[80] though slightly lower than those of chitosan-based systems (reported EE% up to 75%).[78,79] In contrast, the lower EE% and adsorption capacity for nedaplatin (13%, 236 mg g^{-1}) suggest weaker interaction with the CuO surface, which is consistent with both the minimal reduction in the pore volume observed by the BET method and the lower adsorption energy calculated by DFT in this study. This is also lower than values reported for biologically synthesized CuO NPs (EE% 70%, adsorption capacity 850 mg g^{-1})[14] and PEGylated chitosan NPs (EE% 45%, adsorption capacity 720 mg g^{-1}).[41] Overall, these results highlight the potential of CuO nanoparticles as robust and efficient carriers for platinum-based drugs, particularly cisplatin, and support their further development for targeted anticancer drug delivery (Table 2).

Drug release profile

The *in vitro* release profiles of cisplatin, oxaliplatin, and nedaplatin from CuO nanoparticles were evaluated in phosphate buffer (pH 7.4) at 37.5 °C over 72 hours. The cumulative percentage of drugs released was measured at predetermined time intervals using UV-vis spectroscopy. The results (Fig. 10)

Table 2 Comparative entrapment efficiency and adsorption capacity of Pt(II) drug-loaded nanoparticles

Drug	Nanoparticle carrier	Entrapment efficiency (EE%)	Adsorption capacity (mg g^{-1})	Ref.
Cisplatin	CuO NPs	52	949	This work
Cisplatin	CuO NPs	52	949	This work
Oxaliplatin	CuO NPs	38	878	This work
Nedaplatin	CuO NPs	13	236	This work
Nedaplatin	CuO NPs	70	850	14
Nedaplatin	PEGylated chitosan NPs	45	720	41
Cisplatin	PLGA-mPEG NPs	30–40	~200	42
Cisplatin	PBCA NPs	23	Not reported	67
Cisplatin	Polymeric micelles	60	450	40
Oxaliplatin	Mesoporous silica NPs, chitosan	75, 15	650	78 and 79
Cisplatin	Liposomes	85	Not reported	8

Open Access Article. Published on 10 July 2025. Downloaded on 2/8/2026 3:01:31 PM.
This article is licensed under a Creative Commons Attribution 3.0 Unported Licence.

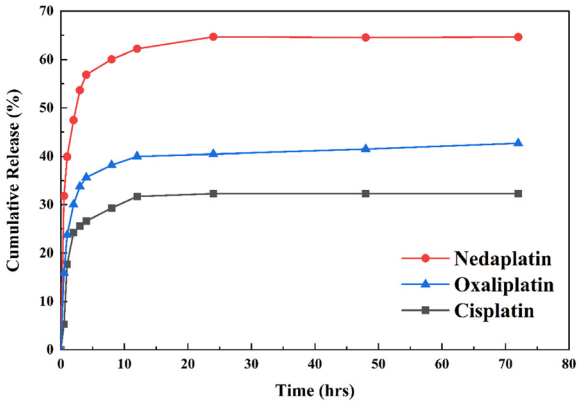

Fig. 10 Cumulative drug release profile of cisplatin, oxaliplatin, and nedaplatin.

show a sustained and controlled release for all three drugs, with cisplatin exhibiting the slowest release (~32% at 72 h), oxaliplatin intermediate (~42%), and nedaplatin the fastest (~65%), compared to rapid release from free drugs. This controlled release behavior is attributed to the strong drug–carrier interactions demonstrated by DFT and correlates with the entrapment efficiency and adsorption capacity discussed above.

This controlled release behavior aligns with previous literature reports. For instance, Ghaferi *et al.* (2020) observed 76% release of free cisplatin within the first hour compared to 28% from cisplatin-loaded PBCA nanoparticles.[67] Similarly, cisplatin-loaded albumin nanoparticles demonstrated sustained release compared to free cisplatin (80% release in 45 hours).[81] We have illustrated a comparison with the literature in Fig. 11. The observed controlled release from our cisplatin–CuO system suggests favorable drug–carrier interactions, which is consistent with our DFT calculations showing a strong binding energy (−3.0 eV) between cisplatin and the CuO surface.

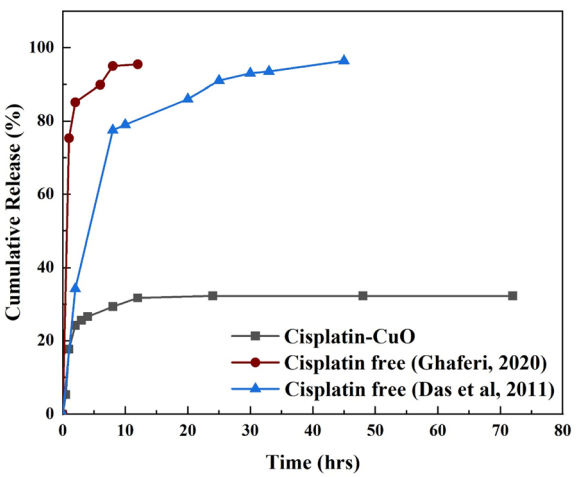

Fig. 11 A comparison between the drug release profile of the free cisplatin drug and loaded cisplatin.

Interaction between the Pt(II)-drugs and CuO NPS: DFT calculations

DFT calculations were performed to investigate the interaction between cisplatin (cis), nedaplatin (neda) and oxaliplatin (oxa) and the CuO(111) surface. The adsorption of Pt(II)-based drugs was also evaluated considering the presence of an –OH functional group, according to the experimental evidence reported in Fig. 3. The most stable configurations of the Pt(II)-drugs on CuO(111) and CuO(111)@OH (Fig. 12) were obtained by considering different coordination modes of the drugs on CuO(111) and calculating the adsorption energies (E_{ads}, eV) of cis, neda and oxa for each configuration, according to eqn (1).

The adsorption energy of the most stable interaction between cisplatin and the CuO(111) surface is found to be −3.0 eV (see cis@CuO(111) in Fig. 12A). In the cis@CuO(111) structure, the chlorine atoms of cisplatin coordinate with the tri-coordinated Cu_1 of the surface layer (for definition see Fig. 2), forming two new Cu_1–Cl bonds of 2.3 Å. In fact, it is known that the coordination at the tri-coordinate Cu site (Cu_1) is energetically more favorable than that at the tetra-coordinate one (Cu_2) as Cu_1 is coordinatively unsaturated, whereas Cu_2 is coordinatively saturated.[54]

The adsorption energy associated with this structure is enhanced by the formation of two hydrogen bonds between the amine ligands (–NH_3) of the drug and the surface oxygen atoms O_1 (for definition see Fig. 2) of 1.7 Å (Fig. 12A).

In the most stable structure of neda@CuO(111) (Fig. 12B), an oxygen atom of the glycolate bidendate ligand, indicated $O1_{neda}$, interacts with CuO(111) through the formation of an $O1_{neda}$–Cu_1 bond of 2.0 Å. The formation of two additional hydrogen bonds between the amine groups (–NH_3) of the drug and the surface O_1 atoms of 1.7 and 1.8 Å, respectively, leads to a negative adsorption energy (−2.6 eV) highlighting a favorable adsorption process of the drug.

Fig. 12C shows the most stable structure of the oxaliplatin adsorbed on CuO(111) (oxa@CuO(111)). In oxa@CuO(111), the metal center Pt forms a 2.7 Å long bond with the surface tri-coordinated Cu_1. In addition, the coordination is further stabilized through H-bonds between the bidentate diaminocyclohexane ligand and the surface O_1 atoms of 1.6 and 1.7 Å, respectively. The adsorption energy associated with this structure is −2.8 eV.

In the presence of the –OH functional group, whose coordination is thermodynamically favored at the Cu_1 site over Cu_2 by 0.4 eV, in line with the previously discussed rationale, the adsorption energies of cisplatin, nedaplatin and oxaliplatin are improved by about 0.5, 1.0, and 0.2 eV, respectively (compare E_{ads} in Fig. 12 panels A–C and A′–C′). In the case of cisplatin and oxaliplatin, the adsorption energies, −3.5 and 3.0 eV, respectively, are further stabilized by H-bonds involving one of the two cisplatin amino groups (–NH_3), the oxaliplatin diaminocyclohexane ligand and the surface –OH group, of lengths between 2.2 and 2.3 Å (see the H-bond distance in purple in Fig. 12 panels A′ and C′, respectively).

In the nedaplatin case, a strong H-bond between one of the nedaplatin amino groups (–NH_3) and the surface –OH group

 This journal is © The Royal Society of Chemistry 2025

Open Access Article. Published on 10 July 2025. Downloaded on 2/8/2026 3:01:31 PM.
This article is licensed under a Creative Commons Attribution 3.0 Unported Licence.

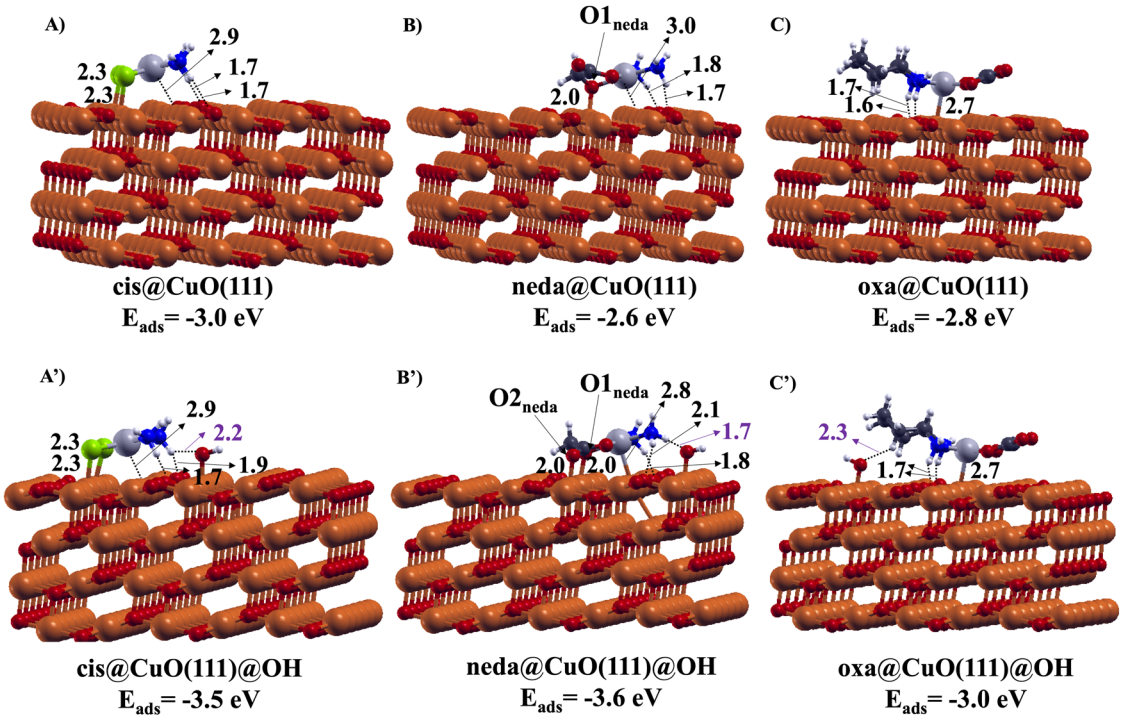

Fig. 12 Optimized geometries related to the interaction of cisplatin, nedaplatin and oxaliplatin with CuO(111) (panels A–C) and CuO(111)@OH (panels A′–C′) and the corresponding E_{ads} (eV). Cu, O, Cl, Pt, C, H and N atoms are represented in ball and sticks and depicted in auburn, red, green, gray, black, white and blue, respectively.

(see the H-bond distance in purple in Fig. 12B′) promotes closer proximity of the drug to the surface. As a result, the nedaplatin adsorption energy is significantly stabilized by the formation of an additional bond between the oxygen atom of the glycolate bidentate ligand – $O2_{neda}$ – and the Cu_1 site of the surface, whose length is equal to that of the $O1_{neda}$–Cu_1 bond, namely 2.0 Å (Fig. 12B′). This additional O–Cu bond aligns the adsorption energy of nedaplatin with that observed for cisplatin (compare the E_{ads} values of cisplatin and nedaplatin in Fig. 12 panels A′ and B′, respectively).

The Pt-drugs have good interaction with the CuO(111) and CuO(111)@OH surfaces, and based on the computed E_{ads} values cisplatin shows the highest binding energy, in agreement with the experimental trends.

Since the Bader charge analysis performed on the systems shown in Fig. 12 did not reveal significant charge transfer (Δq values ranging 0.1–0.2 $|e^-|$), the enhanced adsorption of cisplatin can be attributed exclusively to structural factors. Upon interaction with CuO(111) and CuO(111)@OH, the chlorine atoms of cisplatin form bonds with Cu_1 surface sites, which exhibit a more covalent character compared to those formed between the same sites and the oxygen atoms of nedaplatin. Additionally, Cu_1–Cl bonds in cisplatin are more polarizable than the Cu_1–O bond(s) observed in nedaplatin, due to the distinct electronic properties of the chlorine atom.

On the CuO(111) surface, the adsorption of cisplatin is stronger than that of nedaplatin and oxaliplatin as, in addition to forming hydrogen bonds with the support - similarly to the other two complexes - cisplatin establishes two Cu_1-Cl bonds, whereas nedaplatin forms only a single Cu_1–O bond and oxaliplatin interacts with the surface exclusively through its metal center.

Platinum(II) complexes are well known for their high susceptibility to hydrolysis under physiological conditions. Based on the experimental conditions employed, a further computational investigation was carried out in order to simulate and quantify the adsorption of the hydrolysis products of cisplatin, nedaplatin, and oxaliplatin - indicated as cis(OH)(OH), neda(OH)(H_2O), and oxa(OH)(OH), respectively - on CuO(111) and CuO(111)@OH surfaces. The aim is to evaluate the impact of hydrolysis on drugs adsorption and to determine if this process facilitates or hinders the interaction between Pt(II) drugs and the considered supports. The most stable configurations related to the adsorption of the cisplatin, nedaplatin, and oxaliplatin hydrolysis products on CuO(111) and CuO(111)@OH surfaces, along with the corresponding adsorption energies, are shown in Fig. 13.

The adsorption of the hydrolysis products of cis-, neda-, and oxaliplatin on the CuO(111) surface is significantly more favorable compared to that of the non-hydrolyzed drugs, suggesting that the aquation process enhances the interaction between Pt(II) complexes and the CuO(111) surface (compare E_{ads} reported in Fig. 12 and 13 panels A–C).

In particular, the interaction between the hydrolyzed cisplatin and the metal–oxide support is stabilized by the formation of two Cu_1–OH bonds, with lengths of 2.0 and 1.9 Å (Fig. 13A). Additionally, the associated adsorption energy of −3.5 eV is further stabilized by H-bonds between the amine ligands

Open Access Article. Published on 10 July 2025. Downloaded on 2/8/2026 3:01:31 PM.
This article is licensed under a Creative Commons Attribution 3.0 Unported Licence.

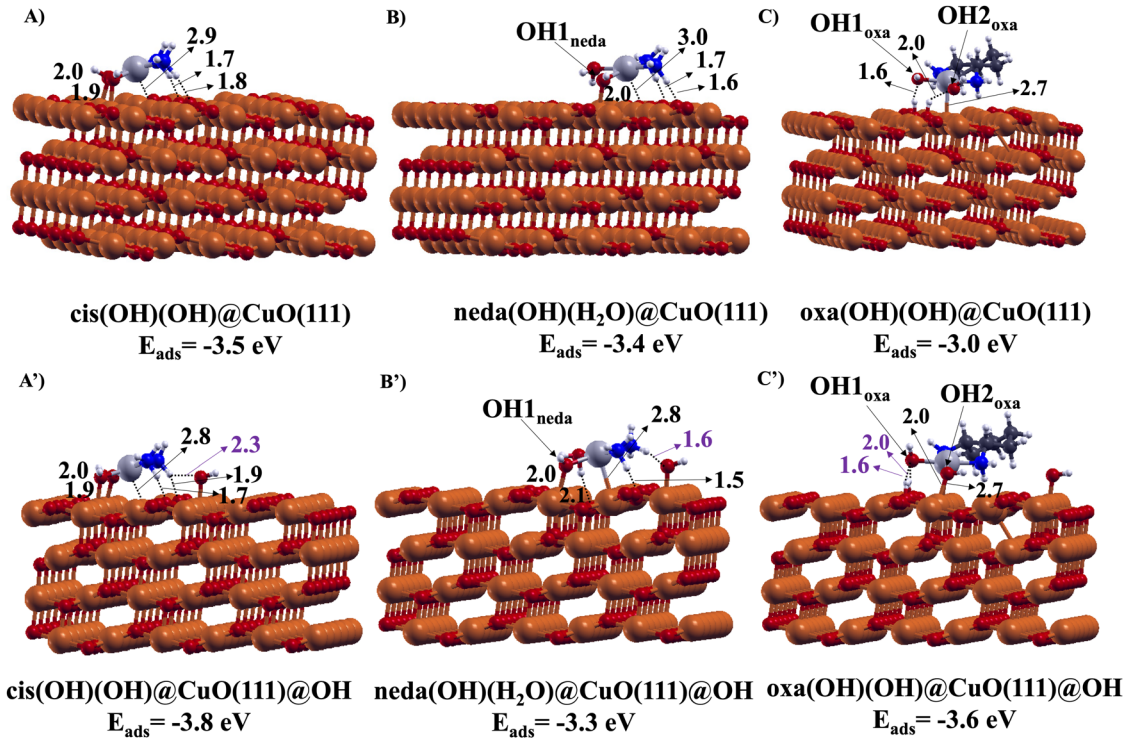

Fig. 13 Optimized geometries related to the interaction of the hydrolysis products of cisplatin, nedaplatin and oxaliplatin with CuO(111) (panels A–C) and CuO(111)@OH (panels A′–C′) and the corresponding E_{ads} (eV). Cu, O, Cl, Pt, C, H and N atoms are represented using a ball and stick model and depicted in auburn, red, green, gray, black, white and blue, respectively.

($-NH_3$) of the hydrolyzed product and the surface oxygen atoms O_1 of 1.7 and 1.8 Å (Fig. 13A).

After the hydrolysis process, the adsorption energy of nedaplatin is very similar to that of the hydrolyzed cisplatin (compare E_{ads} values of −3.5 and −3.4 eV in Fig. 13, panels A and B, respectively). This result is not unexpected, as the hydrolysis products of cisplatin and nedaplatin are structurally very similar. Consequently, the interaction between hydrolyzed nedaplatin and the CuO(111) surface is stabilized by the same factors previously described for cis(OH)(OH), *i.e.*, the formation of a single Cu_1–OH bond, with a length of 2.0 Å, and H-bonds between the amine ligands ($-NH_3$) of the drug and the surface oxygen atoms O_1 of 1.7 and 1.6 Å (Fig. 13B).

Also in this case, among the three drugs considered, oxaliplatin exhibits the weakest adsorption. Its adsorption energy is 0.5 and 0.4 eV less stable than those of cis(OH)(OH) and neda(OH)(H_2O), respectively (compare E_{ads} reported in Fig. 13, panels A–C). Similar to the non-hydrolyzed form, the interaction with CuO(111) involves the formation of a Cu_1–Pt bond, with a length of 2.7 Å (Fig. 13C). However, following hydrolysis, the adsorption is further stabilized by the formation of two H-bonds between the –OH groups of the hydrolyzed drug and two surface protons (H^+), resulting from the dissociation of the two water ligands coordinated to hydrolyzed oxaliplatin. The lengths of these hydrogen bonds are 1.6 and 2.0 Å, respectively (Fig. 13C).

The presence of the –OH functional group enhances the adsorption of the hydrolysis products of cisplatin and oxaliplatin on the CuO(111) surface by 0.3 and 0.6 eV, respectively, while it does not affect the adsorption energy of the hydrolyzed form of nedaplatin (compare E_{ads} in Fig. 13 panels A–C and A′–C′). The interaction of *cis*(OH)(OH) with the CuO(111)@OH surface is further stabilized by H-bonds between one of its amine groups (NH_3) and the surface –OH group, with a length of 2.3 Å (see the H-bond distance in purple in Fig. 13A′). In the case of oxa(OH)(OH), stabilization arises from the formation of a new Cu_1–$OH2_{oxa}$ bond of 2.7 Å (Fig. 13C′). Note that the presence of the –OH functional group does not influence the adsorption of the hydrolyzed product of nedaplatin on the CuO(111)@OH surface (Fig. 13B′).

The adsorption energies reported in Fig. 13 indicate that the hydrolysis process enhances the interaction between the Pt(II)-based drugs and the two supports (compare E_{ads} in Fig. 13 and in Fig. 12). On the CuO(111) surface, the hydrolyzed cisplatin and nedaplatin exhibit very similar adsorption energies (3.5 and 3.4 eV, respectively), which are more favorable than that of oxaliplatin by 0.5 and 0.4 eV, respectively (Fig. 13 panels A–C).

The differences in the hydrolyzed drugs' adsorption behavior are particularly pronounced in the case of the CuO(111)@OH surface, where the strongest interaction is observed for cis(OH)(OH), with an adsorption energy of −3.8 eV, followed by the hydrolyzed products of oxaliplatin (E_{ads} of −3.6 eV) and nedaplatin (E_{ads} of −3.3 eV). This trend is consistent with the drug release profiles reported in Fig. 10.

 This journal is © The Royal Society of Chemistry 2025

Open Access Article. Published on 10 July 2025. Downloaded on 2/8/2026 3:01:31 PM. This article is licensed under a Creative Commons Attribution 3.0 Unported Licence.

Also in this case, Bader charge analysis performed on the models shown in Fig. 13 revealed no significant charge transfer from the Pt(II)-drugs to support and/or *vice versa*. Therefore, the enhanced adsorption energies of the hydrolyzed drugs can be attributed solely to structural factors, namely the formation of bonds and hydrogen interactions between the drugs and the CuO(111) and CuO(111)@OH surfaces.

Conclusion

The experimental results provided valuable data on the surface properties, pore structure, and drug-loading efficiency of the CuO nanoparticles as carriers for Pt(II)-based anticancer drugs. Cisplatin and oxaliplatin showed efficient adsorption on the surface of the CuO nanoparticles by providing a considerable reduction of the surface area and pore volume of CuO as revealed by the BET and BJH measurements. Quantitative UV-vis analysis showed that cisplatin exhibited the highest entrapment efficiency (EE%) at 52% and the greatest adsorption capacity (949 mg g^{-1}), outperforming oxaliplatin (EE% 38%, 878 mg g^{-1}) and nedaplatin (EE% 13%, 236 mg g^{-1}). The experimental results are in line with the DFT calculations according to which Pt(II)-drugs show favorable adsorption on the CuO(111) surface, especially when the Pt(II)-drug is cisplatin. The most stable configurations suggest that cisplatin, nedaplatin and oxaliplatin prefer to coordinate with the surface tri-coordinated Cu. DFT calculations show that all three Pt(II) drugs favorably adsorb on the CuO(111) surface, with cisplatin showing the strongest interaction (adsorption energy up to −3.5 eV in the presence of surface –OH groups). The most stable configurations involve coordination to tri-coordinated surface Cu atoms and, for cisplatin and its hydrolyzed form, the formation of multiple strong bonds and hydrogen interactions. Hydrolysis further enhances the adsorption of all drugs, particularly aligning the energies of cisplatin and nedaplatin, but cisplatin remains the most robustly bound in both experimental and theoretical assessments. *In vitro* release profiles demonstrated sustained and controlled release for all three drugs, with cisplatin exhibiting the slowest release (~32% at 72 h), oxaliplatin intermediate (~42%), and nedaplatin the fastest (~65%). This trend mirrors the strength of drug–carrier interactions and correlates with the entrapment efficiency and DFT-predicted binding energies.

Author contributions

The manuscript was written through contributions from all authors. All authors have given approval to the final version of the manuscript.

Conflicts of interest

The authors declare no competing financial interest.

Data availability

The data supporting this article have been included as part of the ESI.†

Acknowledgements

I. R. and M. F. C. would like to thank the Supercomputing Centre CINECA, Bologna, Italy, for providing computing time under the project IsB25_FORECAST.

References

1 B. Desoize and C. Madoulet, Particular aspects of platinum compounds used at present in cancer treatment, *Crit. Rev. Oncol. Hematol.*, 2002, **42**(3), 317–325, DOI: **10.1016/s1040-8428(01)00219-0**.
2 (*a*) B. Rosenberg, L. Vancamp, J. E. Trosko and V. H. Mansour, Platinum Compounds: a New Class of Potent Antitumour Agents, *Nature*, 1969, **222**, 385–386, DOI: **10.1038/222385a0**; (*b*) B. Rosenberg, L. Vancamp and T. Krigas, Inhibition of Cell Division in *Escherichia coli* by Electrolysis Products from a Platinum Electrode, *Nature*, 1965, **205**, 698–699, DOI: **10.1038/205698a0**.
3 (*a*) Z. H. Siddik, Cisplatin: mode of cytotoxic action and molecular basis of resistance, *Oncogene*, 2003, **22**, 7265–7279, DOI: **10.1038/sj.onc.1206933**; (*b*) M. E. Alberto, V. Butera and N. Russo, Which One among the Pt-Containing Anticancer Drugs More Easily Forms Monoadducts with G and A DNA Bases? A Comparative Study among Oxaliplatin, Nedaplatin, and Carboplatin, *Inorg. Chem.*, 2011, **50**(15), 6965–6971, DOI: **10.1021/ic200148n**.
4 H. Wang, S. Guo, S. J. Kim, F. Shao, J. W. K. Ho, K. U. Wong, Z. Miao, D. Hao, M. Zhao, J. Xu, J. Zeng, K. H. Wong, L. Di, A. H. Wong, X. Xu and C. X. Deng, Cisplatin prevents breast cancer metastasis through blocking early EMT and retards cancer growth together with paclitaxel, *Theranostics*, 2011, **11**(5), 2442–2459, DOI: **10.7150/thno.46460**.
5 W. Jiang, Y. Yan, M. Chen, G. Luo, J. Hao, J. Pan, S. Hu, P. Guo, W. Li, R. Wang, Y. Zuo, Y. Sun, S. Sui, W. Yu, Z. Pan, K. Zou, Z. Zheng, W. Deng, X. Wu and W. Guo, Aspirin enhances the sensitivity of colon cancer cells to cisplatin by abrogating the binding of NF-κB to the COX-2 promoter, *Aging*, 2020, **12**(1), 611–627, DOI: **10.18632/aging.102644**.
6 Y. Y. Kim, W. O. Kim, H. C. Liu, Z. Rosenwaks, J. W. Kim and S. Y. Ku, Effects of paclitaxel and cisplatin on *in vitro* ovarian follicle development, *Arch. Med. Sci.*, 2019, **15**(6), 1510–1519, DOI: **10.5114/aoms.2019.81730**.
7 M. Shimada, H. Itamochi and J. Kigawa, Nedaplatin: a cisplatin derivative in cancer chemotherapy, *Cancer Manage. Res.*, 2013, **5**, 67–76, DOI: **10.2147/cmar.s35785**.
8 C. Zhang, C. Xu, X. Gao and Q. Yao, Platinum-based drugs for cancer therapy and anti-tumor strategies, *Theranostics*, 2022, **12**(5), 2115–2132, DOI: **10.7150/thno.69424**.
9 E. M. Moustafa, I. Ritacco, E. Sicilia, N. Russo and T. Shoeib, Collision-induced dissociation products of the protonated

Open Access Article. Published on 10 July 2025. Downloaded on 2/8/2026 3:01:31 PM. This article is licensed under a Creative Commons Attribution 3.0 Unported Licence.

dipeptide carnosine: structural elucidation, fragmentation pathways and potential energy surface analysis, *Phys. Chem. Chem. Phys.*, 2015, **17**, 12673–12682, DOI: 10.1039/C5CP00958H.

10 I. Ritacco, E. M. Moustafa, E. Sicilia, N. Russo and T. Shoeib, Fragmentation pathways analysis for the gas phase dissociation of protonated carnosine-oxaliplatin complexes, *Dalton Trans.*, 2015, **44**, 4455–4467, DOI: 10.1039/C4DT02217C.

11 I. Ritacco, M. Korany, T. Shoeib, N. Russo and E. Sicilia, Mass Spectrometric and Computational Investigation of the Protonated Carnosine–Carboplatin Complex Fragmentation, *Inorg. Chem.*, 2015, **54**(16), 7885–7897, DOI: 10.1021/acs.inorgchem.5b00959.

12 I. Ritacco, M. Al Assy, M. K. A. El-Rahman, S. A. Fahmy, N. Russo, T. Shoeib and E. Sicilia, Hydrolysis in Acidic Environment and Degradation of Satraplatin: A Joint Experimental and Theoretical Investigation, *Inorg. Chem.*, 2017, **56**, 6013–6026, DOI: 10.1021/acs.inorgchem.7b00945.

13 I. Ritacco, G. Mazzone, N. Russo and E. Sicilia, Investigation of the inertness to hydrolysis of platinum (IV) prodrugs, *Inorg. Chem.*, 2016, **55**(4), 1580–1586, DOI: 10.1021/acs.inorgchem.5b02484.

14 N. M. Aboeita, S. A. Fahmy, M. M. H. El-Sayed, H. M. El-Said Azzazy and T. Shoeib, Enhanced anticancer activity of nedaplatin loaded onto copper nanoparticles synthesized using red algae, *Pharmaceutics*, 2022, **14**(2), 418, DOI: 10.3390/pharmaceutics14020418.

15 M. I. Nabila and K. Kannabiran, Biosynthesis, characterization and antibacterial activity of copper oxide nanoparticles (CuO NPs) from actinomycetes, *Biocatal. Agric. Biotechnol.*, 2018, **15**, 56–62, DOI: 10.1016/j.bcab.2018.05.011.

16 S. P. Selvaraj, Enhanced surface morphology of copper oxide (CuO) nanoparticles and its antibacterial activities, *Mater. Today*, 2022, **50**, 2865–2868, DOI: 10.1016/j.matpr.2020.09.574.

17 M. Chevallet, G. Veronesi, A. Fuchs, E. Mintz, I. Michaud-Soret and A. Deniaud, Impact of labile metal nanoparticles on cellular homeostasis. Current developments in imaging, synthesis and applications, *Biochim. Biophys. Acta, Gen. Subj.*, 2017, **1861**(6), 1566–1577, DOI: 10.1016/j.bbagen.2016.12.012.

18 S. Naz, H. Shahzad, A. Ali and M. Zia, Nanomaterials as nanocarriers: a critical assessment why these are multichore vanquisher in breast cancer treatment, *Artif. Cells, Nanomed., Biotechnol.*, 2018, **46**(5), 899–916, DOI: 10.1080/21691401.2017.1375937.

19 H. R. Naika, K. Lingaraju, K. Manjunath, D. Kumar, G. Nagaraju, D. Suresh and H. Nagabhushana, Green synthesis of CuO nanoparticles using Gloriosa superba L.extract and their antibacterial activity, *J. Taibah Univ. Sci*, 2015, **9**(1), 7–12, DOI: 10.1016/j.jtusci.2014.04.006.

20 S. A. Abdulateef, M. Z. MatJafri, A. F. Omar, N. M. Ahmed, S. A. Azzez, I. M. Ibrahim and B. E. Al-Jumaili, Preparation of CuO nanoparticles by laser ablation in liquid, *AIP Conf. Proc.*, 2016, **1733**, 020035, DOI: 10.1063/1.4948853.

21 M. Devaraji, P. V. Thanikachalam and K. Elumalai, The potential of copper oxide nanoparticles in nanomedicine: a comprehensive review, *Biotechnol. Notes*, 2024, **5**, 80–99, DOI: 10.1016/j.biotno.2024.06.001.

22 L. E. Garcia-Marin, K. Juarez-Moreno, A. R. Vilchis-Nestor and E. Castro-Longoria, Highly Antifungal Activity of Biosynthesized Copper Oxide Nanoparticles against *Candida albicans*, *Nanomaterials*, 2022, **12**(21), 3856, DOI: 10.3390/nano12213856.

23 G. Applerot, J. Lellouche, A. Lipovsky, Y. Nitzan, R. Lubart, A. Gedanken and E. Banin, Understanding the antibacterial mechanism of CuO nanoparticles: revealing the route of induced oxidative stress, *Small*, 2012, **8**(21), 3326–3337, DOI: 10.1002/smll.201200772.

24 M. Shafagh, F. Rahmani and N. Delirezh, CuO nanoparticles induce cytotoxicity and apoptosis in human K562 cancer cell line *via* mitochondrial pathway, through reactive oxygen species and P53, *Iran. J. Basic Med. Sci.*, 2015, **18**(10), 993–1000PMID: 26730334; PMCID: PMC4686584.

25 S. Naz, A. Gul and M. Zia, Toxicity of copper oxide nanoparticles: a review study, *IET Nanobiotechnol.*, 2020, **14**(1), 1–13, DOI: 10.1049/iet-nbt.2019.0176.

26 A. Wongrakpanich, I. A. Mudunkotuwa, S. M. Geary, A. S. Morris, K. A. Mapuskar, D. R. Spitz, V. H. Grassian and A. K. Salem, Size-dependent cytotoxicity of copper oxide nanoparticles in lung epithelial cells, *Environ. Sci.: Nano*, 2016, **3**, 365–374, DOI: 10.1039/c5en00271k.

27 E. Moschini, G. Colombo, G. Chirico, G. Capitani, I. Dalle-Donne and P. Mantecca, Biological mechanism of cell oxidative stress and death during short-term exposure to nano CuO, *Sci. Rep.*, 2023, **13**(1), 2326, DOI: 10.1038/s41598-023-28958-6.

28 S. S. Ahmed and N. Abbass, Synthesis and Anticancer Activity of Polymer Nanocomposites with Moringa-Extracted CuO and Ag_2O Nanoparticles, *Rep. Biochem. Mol. Biol.*, 2024, **13**(3), 405–419, DOI: 10.61186/rbmb.13.3.405.

29 C. D. Tran, J. Makuvaza, E. Munson and B. Bennett, Biocompatible copper oxide nanoparticle composites from cellulose and chitosan: facile synthesis, unique structure, and antimicrobial activity, *ACS Appl. Mater. Interfaces*, 2017, **9**(49), 42503–42515, DOI: 10.1021/acsami.7b11969.

30 L. Wang, C. Hu and L. Shao, The antimicrobial activity of nanoparticles: present situation and prospects for the future, *Int. J. Nanomed.*, 2017, **12**, 1227–1249, DOI: 10.2147/ijn.s121956.

31 S. Jammi, S. Sakthivel, L. Rout, T. Mukherjee, S. Mandal, R. Mitra, P. Saha and T. Punniyamurthy, CuO nanoparticles catalyzed C-N, C-O, and C-S cross-coupling reactions: Scope and mechanism, *J. Org. Chem.*, 2009, **74**(5), 1971–1976, DOI: 10.1021/jo8024253.

32 H. Assefa, S. Singh, N. Shehata, N. A. Khan, F. E. Olu and P. C. Ramamurthy, Green synthesis and characterization of CuO/PANI nanocomposite for efficient Pb (II) adsorption from contaminated water, *Sci. Rep.*, 2024, **14**(1), 30972, DOI: 10.1038/s41598-024-81970-2.

33 C. Angelé-Martínez, K. V. Nguyen, F. S. Ameer, J. N. Anker and J. L. Brumaghim, Reactive oxygen species generation by copper(II) oxide nanoparticles determined by DNA damage assays and EPR spectroscopy, *Nanotoxicology*, 2017, **11**(2), 278–288, DOI: 10.1080/17435390.2017.1293750.

 This journal is © The Royal Society of Chemistry 2025

Open Access Article. Published on 10 July 2025. Downloaded on 2/8/2026 3:01:31 PM. This article is licensed under a Creative Commons Attribution 3.0 Unported Licence.

34 X. Ma, S. Zhou, X. Xu and Q. Du, Copper-containing nanoparticles: Mechanism of antimicrobial effect and application in dentistry-a narrative review, *Front. Surg.*, 2022, **9**, 905892, DOI: **10.3389/fsurg.2022.905892**.

35 B. L. da Silva, B. L. Caetano, B. G. Chiari-Andréo, R. C. L. R. Pietro and L. A. Chiavacci, Increased antibacterial activity of ZnO nanoparticles: Influence of size and surface modification, *Colloids Surf., B*, 2019, **177**, 440–447, DOI: **10.1016/j.colsurfb.2019.02.013**.

36 N. A. A. Yusof, N. M. Zain and N. Pauzi, Synthesis of ZnO nanoparticles with chitosan as stabilizing agent and their antibacterial properties against Gram-positive and Gram-negative bacteria, *Int. J. Biol. Macromol.*, 2019, **124**, 1132–1136, DOI: **10.1016/j.ijbiomac.2018.11.228**.

37 M. Hirota, Y. Sugita, M. Ishijima, T. Ikeda, J. Saruta, H. Maeda and T. Ogawa, UV photocatalytic activity of titanium dioxide (TiO_2) surface contaminated with bacterial biofilm: Implications for photo-restoration of osteoconductivity, *Mater Today Adv.*, 2021, **12**, 10018, DOI: **10.1016/j.mtadv.2021.100182**.

38 C. Ripolles-Avila, M. Martinez-Garcia, A. S. Hascoët and J. J. Rodríguez-Jerez, Bactericidal efficacy of UV activated TiO_2 nanoparticles against Gram-positive and Gram-negative bacteria on suspension, *Cienc. Tecnol. Aliment.*, 2019, **17**(1), 408–418, DOI: **10.1080/19476337.2019.1590461**.

39 M. Agarwala, B. Choudhury and R. N. Yadav, Comparative study of antibiofilm activity of copper oxide and iron oxide nanoparticles against multidrug resistant biofilm forming uropathogens, *Indian J. Microbiol.*, 2014, **54**(3), 365–368, DOI: **10.1007/s12088-014-0462-z**.

40 G. Fang, A. Zhang, L. Zhu, Q. Wang, F. Sun and B. Tang, Nanocarriers containing platinum compounds for combination chemotherapy, *Front. Pharmacol.*, 2022, **13**, 1050928, DOI: **10.3389/fphar.2022.1050928**.

41 S. A. Fahmy, A. Ramzy, N. M. El Samaloty, N. K. Sedky and H. M. W. S. Azzazy, PEGylated Chitosan Nanoparticles Loaded with Betaine and Nedaplatin Hamper Breast Cancer: *In Vitro* and *In Vivo* Studies, *ACS Omega*, 2023, **8**(44), 41485–41494, DOI: **10.1021/acsomega.3c05359**.

42 L. Cheng, C. Jin, W. Lv, Q. Ding and X. Han, Developing a highly stable PLGA-mPEG nanoparticle loaded with cisplatin for chemotherapy of ovarian cancer, *PLoS One*, 2011, **6**(9), e25433.

43 Drawell Analytical. (2024). *Sample preparation for FTIR analysis: Sample types and preparation methods*. Retrieved from **https://www.drawellanalytical.com**.

44 A. Olori, P. Di Pietro and A. Campopiano, Preparation of ultrapure KBr pellet: New method for FTIR quantitative analysis, *Int. J. Sci. Acad. Res.*, 2021, **2**(2), 1015–1020.

45 Cisplatin Datasheet. (n.d.): **https://www.sigmaaldrich.com/deepweb/assets/sigmaaldrich/product/documents/310/148/p4394pis.pdf**.

46 Oxaliplatin Datasheet. (n.d.): **https://www.selleckchem.com/datasheet/Eloxatin-S122415-DataSheet.html**.

47 Nedaplatin. Nedaplatin Datasheet. (n.d.): **https://www.selleckchem.com/datasheet/nedaplatin-aqupla-S182604-DataSheet.html**.

48 J. P. Perdew, K. Burke and M. Ernzerhof, Generalized Gradient Approximation Made Simple, *Phys. Rev. Lett.*, 1996, **77**, 3865, DOI: **10.1103/PhysRevLett.77.3865**.

49 D. Vanderbilt, Soft self-consistent pseudopotentials in a generalized eigenvalue formalism, *Phys. Rev. B: Condens. Matter Mater. Phys.*, 1990, **41**, 7892, DOI: **10.1103/PhysRevB.41.7892**.

50 P. Giannozzi, O. Andreussi, T. Brumme, O. Bunau, M. Buongiorno Nardelli, M. Calandra, R. Car, C. Cavazzoni, D. Ceresoli and M. Cococcioni, *et al.*, Advanced capabilities for materials modelling with QuantumESPRESSO, *J. Phys.: Condens. Matter*, 2017, **29**, 465901, DOI: **10.1088/1361-648X/aa8f79**.

51 J. Hu, D. Li, J. G. Lu and R. Wu, Effects on Electronic Properties of Molecule Adsorption on CuO Surfaces and Nanowires, *J. Phys. Chem. C*, 2010, **114**(40), 17120–17126, DOI: **10.1021/jp1039089**.

52 S. Åsbrink and L.-J. Norrby, A Refinement of the Crystal Structure of Copper (II) Oxide with a Discussion of Some Exceptional Esd's, *Acta Crystallogr., Sect. B*, 1970, **26**(1), 8–15, DOI: **10.1107/S0567740870001838**.

53 V. Massarotti, D. Capsoni, M. Bini, A. Altomare and A. G. G. Moliterni, X-Ray Powder Diffraction *Ab Initio* Structure Solution of Materials from Solid State Synthesis: The Copper Oxide Case, *Z. Kristallogr. - Cryst. Mater.*, 1998, **213**(5), 259–265, DOI: **10.1524/zkri.1998.213.5.259**.

54 X. Yu, X. Zhang, H. Wang and G. Feng, High coverage water adsorption on the CuO(111) surface, *Appl. Surf. Sci.*, 2017, **425**, 803–810, DOI: **10.1016/j.apsusc.2017.07.086**.

55 D. Ma and Z. Cao, Adsorption and Decomposition of Sarin on Dry and Wet Cu_2O(111) and CuO(111) Surfaces: Insight from First-Principles Calculations, *J. Phys. Chem. C*, 2021, **125**, 24396–24405, DOI: **10.1021/acs.jpcc.1c07072**.

56 Y. Guan, W. Suo, Z. Zhang, Y. Wang, S. Sun and G. Liu, Insights on the Catalytic Active Site for CO2 Reduction on Copper-based Catalyst: A DFT study, *Mol. Catal.*, 2021, **511**, 111725, DOI: **10.1016/j.mcat.2021.111725**.

57 A. K. Mishra, A. Roldan and N. H. de Leeuw, CuO Surfaces and CO_2 Activation: A Dispersion-Corrected DFT+U Study, *J. Phys. Chem. C*, 2016, **120**(4), 2198–2214, DOI: **10.1021/acs.jpcc.5b10431**.

58 S. Grimme, J. Antony, S. Ehrlich and H. Krieg, A Consistent and Accurate *Ab Initio* Parametrization of Density Functional Dispersion Correction (DFT-D) for the 94 Elements H-Pu, *J. Chem. Phys.*, 2010, **132**(15), 154104, DOI: **10.1063/1.3382344**.

59 W. Tang, E. Sanville and G. Henkelman, A Grid-Based Bader Analysis Algorithm Without Lattice Bias, *J. Phys.: Condens. Matter*, 2009, **21**(8), 084204, DOI: **10.1088/0953-8984/21/8/084204**.

60 E. Sanville, S. D. Kenny, R. Smith and G. Henkelman, Improved Grid-Based Algorithm for Bader Charge Allocation, *J. Comput. Chem.*, 2007, **28**(5), 899–908, DOI: **10.1002/jcc.20575**.

61 G. Henkelman, A. Arnaldsson and H. Jonsson, A Fast and Robust Algorithm for Bader Decomposition of Charge

Open Access Article. Published on 10 July 2025. Downloaded on 2/8/2026 3:01:31 PM.
This article is licensed under a Creative Commons Attribution 3.0 Unported Licence.

Density, *Comput. Mater. Sci.*, 2006, **36**, 354–360, DOI: 10.1016/j.commatsci.2005.04.010.

62 H. Vaddar, V. D. Jangannanavar, H. Basavanagoudra, P. S. Aratal, M. K. Patil, S. R. Inamdar and K. M. Goudar, Nano-crafting copper oxide: A novel electrode fabrication for enhanced electrochemical tryptophan detection and efficient photodegradation of nile blue dye, *Ceram. Int.*, 2025, **51**(6), 7001–7014, DOI: 10.1016/j.ceramint.2024.12.135.

63 A. R. Aly, A. G. El-Demerdash, W. Sadik, E. El Rafy and T. Shoeib, Upcycling of sugar refining mud solid waste as a novel adsorbent for removing methylene blue and Congo red from wastewater, *RSC Adv.*, 2024, **14**(19), 13505–13520, DOI: 10.1039/D4RA01451K.

64 A. Shafiq, U. Jeong, Y. Han, Y. Kim, J. Lee and B. S. Kim, Green Synthesis of Copper Oxide Nanoparticles from Waste Solar Panels Using *Piper nigrum* Fruit Extract and Their Antibacterial Activity, *Catalysts*, 2024, **14**, 472, DOI: 10.3390/catal14080472.

65 S. G. Ali, U. Haseen, M. Jalal, R. A. Khan, A. Alsalme, H. Ahmad and H. M. Khan, Green Synthesis of Copper Oxide Nanoparticles from the Leaves of *Aegle marmelos* and Their Antimicrobial Activity and Photocatalytic Activities, *Molecules*, 2023, **28**(22), 7499, DOI: 10.3390/molecules28227499.

66 P. K. Raul, S. Senapati, A. K. Sahoo, I. M. Umlong, R. R. Devi, A. J. Thakur and V. Veer, CuO nanorods: a potential and efficient adsorbent in water purification, *RSC Adv.*, 2014, **4**, 40580–40587, DOI: 10.1039/C4RA04619F.

67 M. Ghaferi, S. Amari, B. Vivek Mohrir, A. Raza, H. Ebrahimi Shahmabadi and S. E. Alavi, Preparation, Characterization, and Evaluation of Cisplatin-Loaded Polybutylcyanoacrylate Nanoparticles with Improved *in Vitro* and *in Vivo* Anticancer Activities, *Pharmaceuticals*, 2020, **13**(3), 44, DOI: 10.3390/ph13030044.

68 F. F. Azhar, E. Shahbazpour and A. Olad, pH sensitive and controlled release system based on cellulose nanofibers-poly vinyl alcohol hydrogels for cisplatin delivery, *Fibers Polym.*, 2017, **18**(3), 416–423, DOI: 10.1007/s12221-017-6958-5.

69 E. D. Pereira, R. Cerruti, E. Fernandes, L. Peña, V. Saez, J. C. Pinto, J. A. Ramón, G. E. Oliveira and F. G. de Souza, Influence of PLGA and PLGA-PEG on the Dissolution Profile of Oxaliplatin, *Polímeros*, 2016, **26**(2), 137–143, DOI: 10.1590/0104-1428.2323.

70 M. Torres, S. Khan, M. Duplanty, H. C. Lozano, T. J. Morris, T. Nguyen, Y. V. Rostovtsev, N. J. DeYonker and N. Mirsaleh-Kohan, Raman and infrared studies of platinum-based drugs: cisplatin, carboplatin, oxaliplatin, nedaplatin, and heptaplatin, *J. Phys. Chem. A*, 2018, **122**(34), 6934–6952, DOI: 10.1021/acs.jpca.8b04023.

71 E. Badetti, L. Calgaro, L. Falchi, A. Bonetto, C. Bettiol, B. Leonetti, E. Ambrosi, E. Zendri and A. Marcomini, Interaction between copper oxide nanoparticles and amino acids: influence on the antibacterial activity, *Nanomaterials*, 2019, **9**(5), 792, DOI: 10.3390/nano9050792.

72 I. Z. Luna, L. N. Hilary, A. S. Chowdhury, M. A. Gafur, N. Khan and R. A. Khan, Preparation and characterization of copper oxide nanoparticles synthesized *via* chemical precipitation method, *OALibJ*, 2015, **2**(3), 1–8, DOI: 10.4236/oalib.1101409.

73 L. Ragunath, J. Suresh, M. Sankaran, R. S. Kumar, A. I. Almansour and N. Arumugam, Synthesis and characterization of copper oxide nanoparticles using rambutan peel extract *via* greener route, *Rasayan J. Chem.*, 2021, **14**(4), 2660–2665, DOI: 10.31788/rjc.2021.1446512.

74 K. S. W. Sing, The Use of Gas Adsorption for the Characterization of Porous Solids, *Colloids Surf.*, 1989, **38**, 113–124, DOI: 10.1016/0166-6622(89)80148-9.

75 A. Samide, R. Grecu, B. Tutunaru, C. Tigae and C. Spînu, Cisplatin-Chemotherapeutic Drug Interactions with the Surface of Some Metal Bioimplants in Physiological Serum, *Int. J. Electrochem. Sci.*, 2017, **12**(12), 11316–11329, DOI: 10.20964/2017.12.66.

76 Y. Lv, H. He, J. Qi, Y. Lu, W. Zhao, X. Dong and W. Wu, Visual Validation of the Measurement of Entrapment Efficiency of Drug Nanocarriers, *Int. J. Pharm.*, 2018, **547**(1–2), 395–403, DOI: 10.1016/j.ijpharm.2018.06.025.

77 E. Drioli and L. Giorno, *Encyclopedia of Membranes*, Springer Berlin Heidelberg, 2016.

78 M. M. Khan, A. Madni, N. Tahir, F. Parveen, S. Khan, N. Jan, A. Ali, M. Abdurrahim, U. Farooq and M. I. Khan, Co-delivery of curcumin and cisplatin to enhance cytotoxicity of cisplatin using lipid-chitosan hybrid nanoparticles, *Int. J. Nanomed.*, 2020, **15**, 2207–2217, DOI: 10.2147/ijn.s247893.

79 K. Trzeciak, A. Chotera-Ouda, I. I. Bak-Sypien and M. J. Potrzebowski, Mesoporous silica particles as drug delivery systems—the state of the art in loading methods and the recent progress in analytical techniques for monitoring these processes, *Pharmaceutics*, 2021, **13**(7), 950, DOI: 10.3390/pharmaceutics13070950.

80 P.-J. Zhang, M.-D. Liu, F.-Y. Fan and K.-X. Liu, A Study on Mesoporous Silica Loaded With Novel Photosensitizers HCE6 and Oxaliplatin for the Treatment of Cholangiocarcinoma, *Front. Oncol.*, 2021, **11**, 665182, DOI: 10.3389/fonc.2021.665182, 34268112.

81 S. Das, L. Jagan, R. Isiah, B. Rajesh, S. Backianathan and J. Subhashini, Nanotechnology in oncology: characterization and: in vitro: release kinetics of cisplatin-loaded albumin nanoparticles: implications in anticancer drug delivery, *Indian J Pharmacol.*, 2011, **43**(4), 409–413, DOI: 10.4103/0253-7613.83111.

 This journal is © The Royal Society of Chemistry 2025